Chapter 12
Studies of Microstructure Properties and Gas Sensing Performance of $(Sn_{0.3}Ti_{0.7})O_2$ Thick Film Resistors

P. D. Hire, V. B. Gaikwad, N. U. Patil, M. K. Deore and G. H. Jain

Abstract In this work we report the synthesis, microstructure, electric properties and sensing performance of $(Sn_{0.3}Ti_{0.7})O_2$ powder, were prepared by wet chemistry route. Thick films were prepared by screen-printing technology. The surfaces of the films were modified by dipping them into an aqueous solution of copper chloride for different intervals of time, followed by firing at 550 °C for 30 min. pure film showed response to CO_2 at 300 °C and cupricated films have been found to be highly selective towards H_2S at 200 °C. The surface modification, using dipping process, altered the adsorbate–adsorbent interactions, which gave the unusual gas response and selectivity effect. The characterization of the films was done by Scanning Electron microscopy, X-ray diffraction, Thermal gravimetric analysis and UV spectrophotometer. Single peaks of the X-ray diffraction pattern reveals that the formation of compound of $(Sn_{0.3}Ti_{0.7})O_2$. Average crystallite size was found to be 41 nm of pure film. The role played by surface copper species in the gas sensing performance is discussed. Grain size, electric properties and gas sensitivity of the films were measured and presented.

Keywords $(Sn_{0.3}Ti_{0.7})O_2(ST_{30})$ · Thick films · H_2S gas sensor · Gas response · Selectivity

P. D. Hire · N. U. Patil · M. K. Deore · G. H. Jain (✉)
Material Research Lab, K.T.H.M. College, Nashik 422002, India
e-mail: gotanjain@rediffmail.com

V. B. Gaikwad
B.C.U.D, University of Pune, Pune 411007, India

A. Mason et al. (eds.), *Sensing Technology: Current Status and Future Trends I*,
Smart Sensors, Measurement and Instrumentation 7, DOI: 10.1007/978-3-319-02318-2_12,

1 Introduction

Gas sensors are used for monitoring and controlling of industrial processes, analysis of gas compositions, for surveillance and many other applications. The development of gas sensor devices with optimized sensitivity and selectivity has been gaining prominence in recent years [1]. Since the demonstration almost 50 years ago, it has been noted that the adsorption of gas on the surface of metal oxides can bring about a significant change in the electrical resistance of the material. There has been a sustained and successful effort to make use of this change for purposes of gas detection. Hydrogen sulphide is a toxic gas, often produced in coal, coal oil and natural gas manufacturing. Therefore, reliable sensors with low cost, low energy consumption, having high sensitivity, selectivity, and operable in a sub ppm range of H_2S are in high demand for environmental safety and industrial control purposes.

Among the metal oxides, tin dioxide and titanium dioxide, due to their chemical and electrical properties, are particularly appealing both for basic research and for a wide variety of possible applications [2]. Tin dioxide is the most common material in gas sensing [3], but it is widely used as transparent conductor and in heterogeneous catalysis. Titanium dioxide is used as a photocatalyst in solar cells, as an optical coating, in gas sensing, etc. Tin dioxide and titanium dioxide are both wide-gap semiconductors, showing several similarities in structural as well as in electronic properties.

One of the most active fields in the sensor research is the exploration of new materials that enable enhanced gas-sensing properties of all the materials currently examined, semiconducting oxides, for example, SnO_2 and TiO_2. These materials are of strong interest, largely because their physical properties are important for promising application as a gas sensor [4–7]. The gas-sensing property for the SnO_2-based sensors is found to be affected dominantly or even controlled by their surfaces [8]. Above 400–500 °C (oxygen losses), the low temperature SnO_2-sensors suffer from a structure instability and poor selectivity [9], while that for the TiO_2-based sensors by their bulk constituents as well and are suited to work at high temperature (1000–1200 °C)[10]. Since the two oxides have distinct gas-sensing behaviors, a combination of them would presumably initiate a new system [11], which might have the gas sensing properties that are not present in either of their bulk oxides was reported in literature [12–14]. The ST_{30} material could be more selective and stable.

The goal of this chapter is the synthesis of ST_{30} materials. More specifically, we aim at better information on: (i) the structure and morphology of the powder (ii) electronic properties and their changes in contact with different gases. Scanning Electron microscopy (SEM), X-ray diffraction (XRD), Thermal gravimetric analysis (TGA) and UV spectrophotometer measurements were adopted to analyze the morphology, the crystalline structure, crystallite size, thermal stability and band gap of sample. Finally, electrical properties and gas sensing properties have been studied.

2 Experimental

2.1 Preparation of Material

The $(Sn_{0.3}Ti_{0.7})O_2$ powder was synthesized via wet-chemistry route from AR-grade starting materials and solvents, used without any further purification [14]. Tin (II) dichloride dihydrate ($SnCl_2.2H_2O$) (0.3 M) (99.8 %, Aldrich) was dissolved in distilled water. Further Titanium chloride III ($TiCl_3$) (0.7 M), containing 15 % HCl (99.8 %, Aldrich) was introduced dropwise into the solution with constant stirring followed by slowly heating it in air at 80 °C. The dried powder was calcinated at 1,000 °C for 6 h to obtain base material ST_{30} [15–17]. Then this powder was ground in an agate pastle–mortor to ensure sufficiently fine particle size.

2.2 Preparation of Thick Films

The thixotropic paste was formulated by mixing the fine powder of ST_{30} with temporary binder as a mixture of organic solvents. The ratio of the inorganic to organic part was kept at 75:25 in formulating the paste. This paste was screen printed on a glass substrate in a desired pattern (1.5 × 0.5 cm) to prepare thick films [18–20]. The films were fired at 550 °C for 30 min in an air atmosphere to remove the residual.

2.3 Modification of Thick Films

The CuO-modified ST_{30} thick films were obtained by dipping them in a 0.01 M aqueous solution of copper chloride ($CuCl_2$) for different intervals of dipping time of 5, 10 and 20 min. These films were dried at 80 °C, followed by firing at 550 °C for 30 min. The films so prepared are termed as 'cupricated' films [21–23].

2.4 Thickness Measurement

The thickness (t) of the film was calculated using a weight-difference method using (1),

$$t = \frac{m}{\rho \times A} \tag{1}$$

where, m is the mass of the film deposited on the substrate in gm, '*A*' the surface area of the film in cm^2 and 'ρ' is the density of deposited material. Average thickness of the film was observed to be 75 μm. The reproducibility of the film thickness was achieved by maintaining the proper rheology and thixotropy of the paste.

3 Structural Properties

3.1 X-ray Diffraction Analysis

To identify the structure and phase purity of the prepared sample, X-ray diffraction analysis (XRD) measurement was carried out. XRD analysis of these powders were carried out in the 20–80° (2θ) range using Cu-Kα (with $\lambda = 1.542$ Å, 40 kV, 30 mA) radiation. Figure 1 showed the X-ray diffraction patterns of ST_{30} thick film. X-ray diffraction analysis at room temperature was carried out to recognize the crystalline phase of ST_{30} powder. ST_{30} solid solution exhibited a rutile-like single phase. It has been possible to observe that the ST_{30} peak position well matched with JCPDS data of rutile TiO_2 (JCPDS No.: 76–0649), allowing us to indirectly verify that the synthesis of the material correctly occurred. The prepared sample shows single phase of the solid solution ST_{30} at calcinations temperature 1,000 °C. This temperature is lower than that required to prepare the material by the solid-state reaction (1,500 °C) [24]. The sharpness of the peaks indicates the polycrystalline nature of the film material.

Table 1 depicts X-ray diffraction analysis of pure ST_{30} Thick Film. The d values were in good agreement with those in the JCPDS for TiO_2 possessing tetragonal structure. The average crystallite size was determined by using Scherrer formula for various identified diffraction peaks [25] and crystallite size was found to be nearly 41 nm.

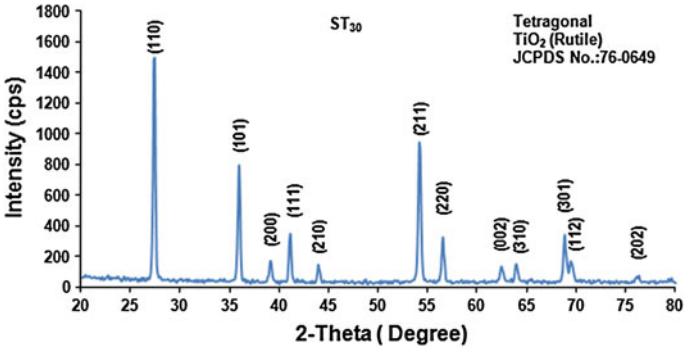

Fig. 1 XRD pattern of pure ST_{30} film

Table 1 X-ray diffraction analysis of pure ST_{30} thick film

Angle (2θ) (°)	d spacing (Å)	FWHM	Peak intensity in %	Crystallite size (nm)	hkl plane
27.40	3.252	0.278	100	42	110
35.87	2.501	0.272	53.1	36	101
39.17	2.298	0.334	11.6	34	200
41.09	2.194	0.280	23.2	42	111
43.89	2.060	0.354	9.8	32	210
54.10	1.693	0.330	62.9	40	211
56.47	1.628	0.274	21.8	48	220
62.32	1.487	0.355	9.1	49	002
63.88	1.445	0.363	10.2	35	310
68.79	1.363	0.291	22.9	49	301
69.42	1.352	0.290	11.3	49	112
76.27	1.247	0.301	4.6	48	202

4 Microstructural Analysis

4.1 Pure ST_{30} Films

Figure 2 depicts a SEM image of a pure ST_{30} thick film fired at 550 °C. The film consists of voids and a wide range of particles with particle sizes ranging from 200 to 840 nm distributed non-uniformly.

4.2 Cupricated ST_{30} Films

Figure 3a–c consist of SEM images of cupricated ST_{30} thick films for the dipping time interval of 05, 10 and 20 min fired at 550 °C, respectively. The micrograph shows a number of small particles distributed uniformly between the larger grains

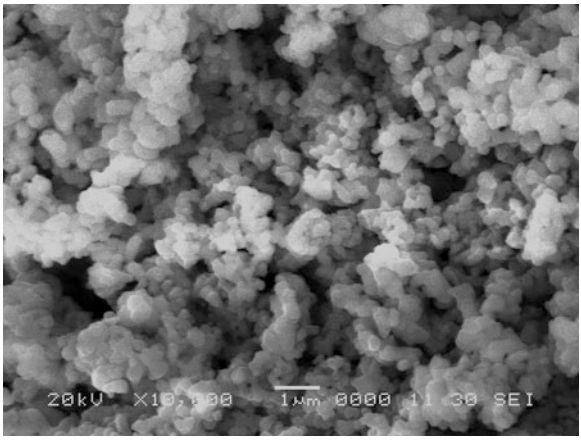

Fig. 2 SEM image of pure ST_{30} films

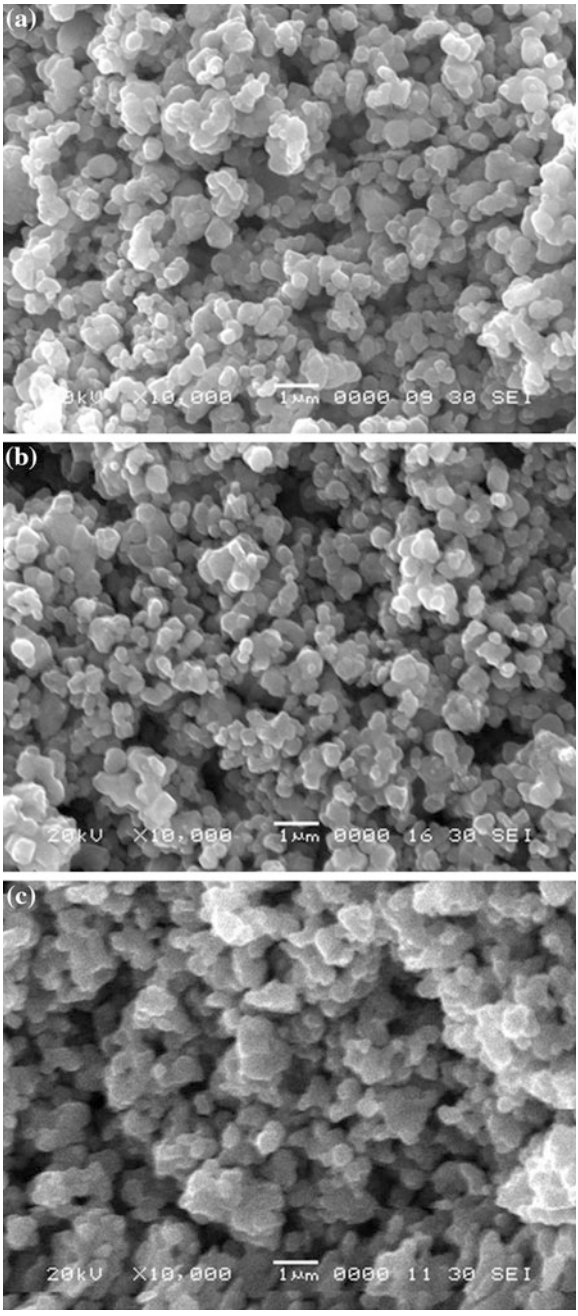

Fig. 3 SEM image of cupricated **a** ST_{30} (05 min), **b** ST_{30} (10 min), and **c** ST_{30} (20 min) films

around the ST_{30} which may be attributed to the presence of CuO. The change in dipping time of the film changes the particle sizes. The particle sizes ranging from 151 to 350 nm (Fig. 3a), 145 to 220 nm (Fig. 3b), and 175 to 500 nm (Fig. 3c) were observed. The micrograph (10 min dipping) appears to consist of a number of small particles distributed uniformly between the larger grains of the ST_{30} film. The smaller particle may be attributed to the presence of CuO. The film seems to be highly porous with a large effective area for oxygen adsorption.

Table 2 depicts the variation of average particle size (d) and specific surface area (SSA) with dipping time of the film. Average particle size (d) was estimated from the SEM images of ST_{30} samples and SSA from (2),

$$A = \frac{6}{\rho \times D} \tag{2}$$

where, ρ is the density of sample and D is the particle size of the films.

5 Elemental Analysis

Figure 4a shows the EDAX spectra of pure ST_{30} film and Fig. 4b shows the EDAX spectra of cupricated ST_{30} films. The quantitative elemental composition of the film and wt % of CuO analysed using an energy dispersive spectrometer are presented in Table 3. It has been observed that the weight percentage of copper increased with dipping time. The film with the dipping time of 10 min was observed to be more oxygen deficient (23.37 wt %). This oxygen deficiency may make the sample possible to adsorb a large amount of oxygen species.

6 Structural Parameters and Their Analysis

6.1 Texture Coefficient

The texture coefficient (Tc) of the film was determined using (3). From that, it was observed that T_C approaches unity for randomly distributed samples whereas T_C is larger than unity for a preferentially oriented (hkl) plane. The lower value of T_C reveals that the films have poor crystallinity. It has been observed that the preferred orientation is the (110) plane for ST_{30} sample. Texture coefficient of the film was found to be 1.13.

Texture coefficient of (hkl) plane,

$$Tc(hkl) = \frac{I(hkl)/Io(hkl)}{\frac{1}{N} \times \sum I(hkl)/Io(hkl)} \tag{3}$$

where, N–No. of planes in XRD pattern.

Table 2 Variation of specific surface area with dipping time of films

Sample	Av. particle size, d nm (SEM)	Specific surface area (SSA) m^2/g
Pure ST_{30} film	520	5.77
Cupricated ST_{30} (05 min)	240	12.50
Cupricated ST_{30} (10 min)	200	15.00
Cupricated ST_{30} (20 min)	337	8.90

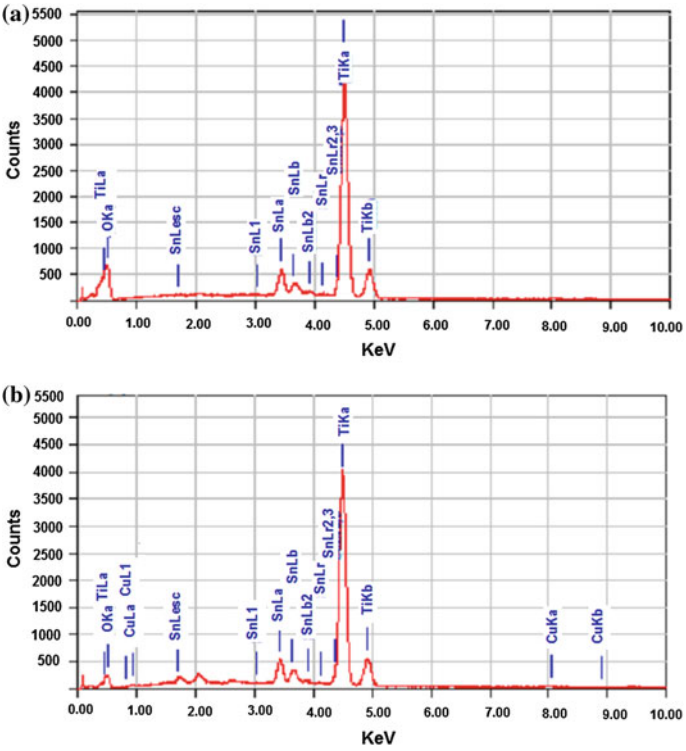

Fig. 4 EDAX spectra of **a** pure ST_{30} and **b** cupricated ST_{30} films

Table 3 Elemental composition of pure and cupricated ST_{30} thick films

Samples	Wt. % of			
	Sn	Ti	O	Cu
Pure ST_{30} film	20.59	49.71	29.70	0.00
Cupricated ST_{30} (05 min)	22.29	51.44	25.91	0.36
Cupricated ST_{30} (10 min)	22.50	52.62	23.37	1.51
Cupricated ST_{30} (20 min)	21.57	51.57	25.25	1.61

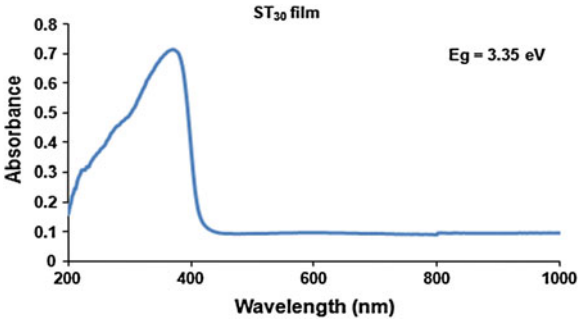

Fig. 5 Diffuse absorbance UV–Vis–NIR spectra of ST_{30}

6.2 UV–Vis–NIR Spectrum Analysis

Figure 5 shows the absorbance spectra of ST_{30} sample. UV analysis of the prepared ST_{30} powder was carried out using JASCO UV–Vis-NIR Spectrophotometer (V-670). The energy band gap, Eg, of the prepared powder was determined using the absorption UV–VIS—NIR spectra. The optical energy band gap was found to be 3.35 eV, using the relationship [26, 27]:

$$Eg = \frac{h \times c}{\lambda} \tag{4}$$

H–Planck's constant, $h = 4.135 \times 10^{-15}$ (eV·s), *c*–speed of light (m/s), $c = 3 \times 10^{8}$ (m/s),

λ–wavelength of light (nm).

7 Thermo Gravimetric Analysis/Differential Thermal Analysis

Figure 6 shows the TGA/DTA profiles of pure ST_{30} sample. Thermogravimetric (TGA) analysis of the samples was carried out using a Mettler Toledo Star system-851 under similar conditions in static air. Thermal stability of pure ST_{30} was examined by a thermo gravimetric analyzer (TGA), using α-Al_2O_3 powder as the reference in air and at a heating rate of 10 °C/min. About 6.008 mg of powders were used for the test. Weight loss ST_{30} material was observed to be nearly 1 %.The small weight loss may be contributing to its larger stability of the prepared material.

The DTA showed the endothermic nature of reactions for pure ST_{30}. The heat absorbed by the samples may be due to the non-stoichiometry of ST_{30} and oxygen deficiency.

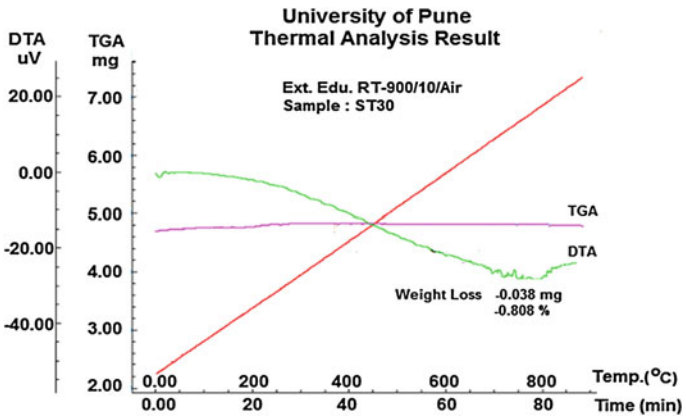

Fig. 6 TGA/DTA of pure ST_{30} material

8 Electrical Properties

8.1 I–V Characteristics

Figure 7 shows the I–V characteristics of pure and cupricated ST_{30} thick films in air atmosphere. The linearity in the graphs indicates the ohmic nature of the pressure contacts.

8.2 Temperature Coefficient of Resistance

Temperature coefficient of resistance for metal is positive, whereas for semiconductors TCR is negative. The relation for resistance and temperature is given by (5),

$$RT = R0[1 + \alpha T] \tag{5}$$

where,

R_T = resistance of sample of temperature T
R_O = resistance of sample at room temperature
T = temperature under consideration
α = TCR of the sample

$$\therefore TCR(\alpha) = \frac{1}{R_o}\left(\frac{\Delta R}{\Delta T}\right) \Big/ {}^{\circ}\mathrm{C}$$

$$\therefore TCR(\alpha) = \frac{\text{slope}}{R_o} \Big/ {}^{\circ}\mathrm{C} \tag{6}$$

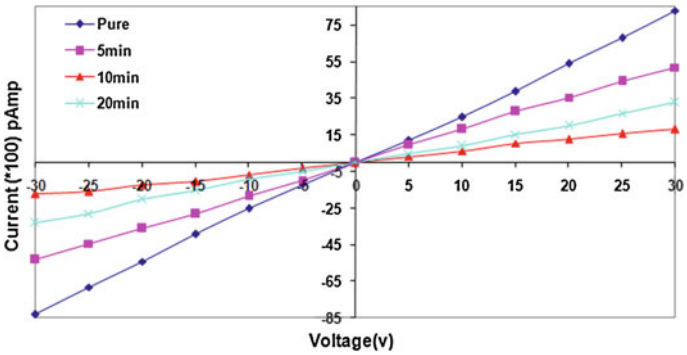

Fig. 7 I-V characteristics of pure and cupricated ST_{30} films

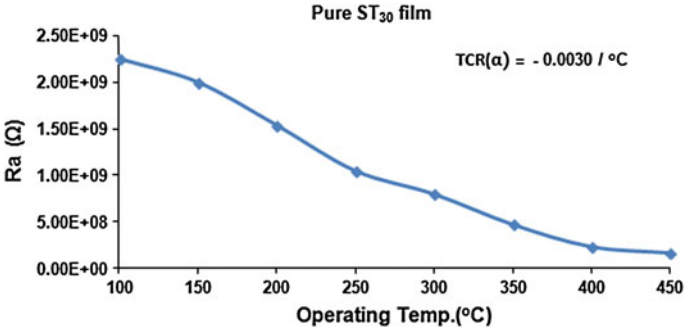

Fig. 8 Variation of resistance of the film with operating temperature

TCR (α) of the pure ST_{30} film was calculated from the slope of the graph of resistance of the film in air (Ra) versus operating temperature (Fig. 8) using (6) and found to be negative. This shows the semiconducting nature of the film.

8.3 Electrical Conductivity

Figure 9 shows the variation of conductivity with temperature for the pure and cupricated samples. The legends suffixed 'a' are the graphs for samples tested in air atmosphere, while the legends suffixed 'g' represent the graphs for the conductivities in the presence of H_2S gas. The graph shows the nonlinear variation of conductivity with temperature for all samples. This shows the semiconducting nature of the films. The conductivity of particular cupricated sample, upon exposure of gas, was larger than that in air. The conductivity of the sample cupricated for 10 min was largest of all. The conductivities of cupricated ST_{30}

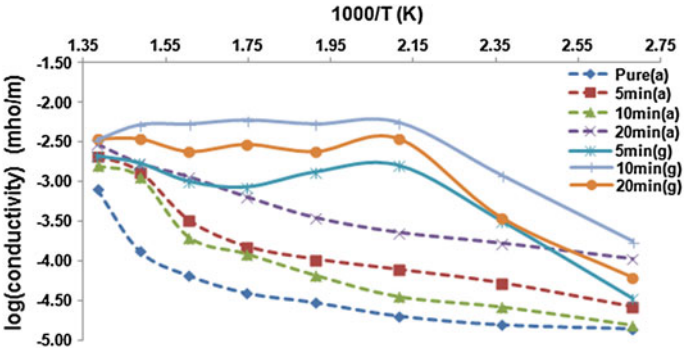

Fig. 9 Variation of electrical conductivity with temperature of pure and cupricated ST_{30} films

Table 4 Variation of activation energy with dipping time ST_{30} thick films

Sample	Activation energy(eV)
Pure ST_{30} film	0.242
Cupricated ST_{30} (05 min)	0.172
Cupricated ST_{30} (10 min)	0.140
Cupricated ST_{30} (20 min)	0.148

samples were larger than that of pure ST_{30} at particular temperature in the presence of gas or in air.

Table 4 represents the activation energy with dipping time of the film, which is calculated from the slope of the graph of log (conductivity) versus 1/T. It has been observed that the activation energy of most sensitive film (10 min.) (0.140 eV) is less than the pure film (0.242 eV) at 300 °C. This reveals that the surface cuprication of the films improves the gas response of the film; since less amount of energy is require to change the one stable state to other state of sensor.

9 Gas Sensing Properties

9.1 Pure ST_{30} Films

9.1.1 Gas Response with Operating Temperature

Figure 10 depicts the response to CO_2 gas with operating temperature of the pure ST_{30} thick films fired at 550 °C.The gas response values of pure thick films were determined at various operating temperatures ranging from 100 to 450 °C for CO_2 gas. The response increases with increasing the operating temperature, attains its maximum at 300 °C and then decreases with a further increase in operating temperature. It has been noted that the optimum operating temperature of pure film is 300 °C.

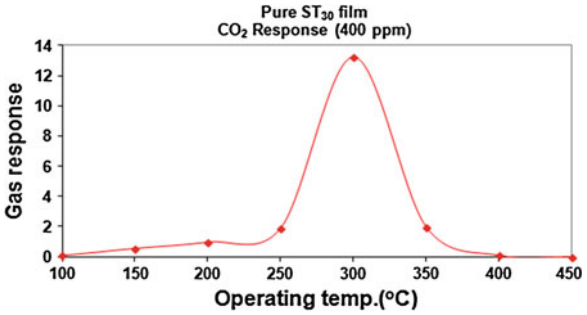

Fig. 10 Variations in response to CO_2 gas with operating temperature of pure ST_{30} film

9.1.2 Selectivity

Figure 11 shows the bar diagram indicating the selectivity of the pure ST_{30} sensor operated at 300 °C to CO_2 gas against other gases. It is evident that the pure sensor is selective to CO_2 at 300 °C gas against the other gases.

9.2 Modified ST_{30} Films

9.2.1 Gas Response with Operating Temperature

The response to H_2S gas with operating temperature of the cupricated ST_{30} thick films for the dipping time interval of 05, 10 and 20 min. fired at 550 °C are represented in Fig. 12.The gas response values of surface cupricated ST_{30} films were determined at various operating temperatures ranging from 100 to 450 °C to H_2S gas. The modified film suppresses gas response of CO_2 gas of pure film and enhances the response to H_2 S gas. The films dipped for 10 min. was most sensitive H_2S gas. The response increases with increasing the operating temperature attains its maximum (at 200 °C) and then decreases with a further increase in operating temperature. It is clear that the optimum operating temperature of cupricated film is 200 °C.

9.2.2 Variation of Gas Response with Dipping Time

Figure 13 shows the variation of the gas response of the cupricated films treated for different intervals of dipping time. It is clear that the response to H_2S goes on increasing with an increase in the dipping time interval. H_2S gas response attains its maximum at 10 min dipping and decreases with further dipping.

9.2.3 Selectivity

Figure 14 depicts the selectivity of the cupricated (10 min) ST_{30} film operated at 200 °C to H_2S gas against other gases. The cupricated film suppresses response of

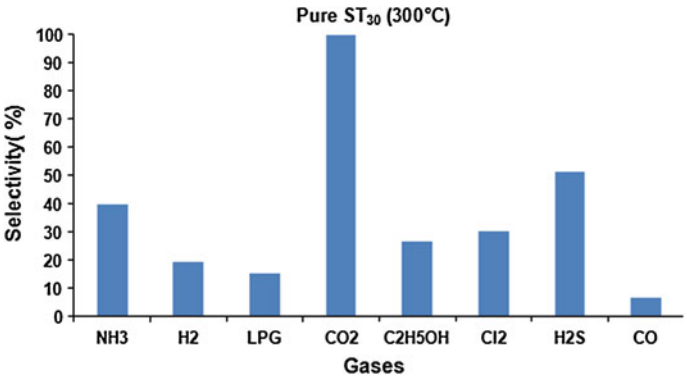

Fig. 11 Selectivity of pure ST_{30} film to CO_2 against other gases

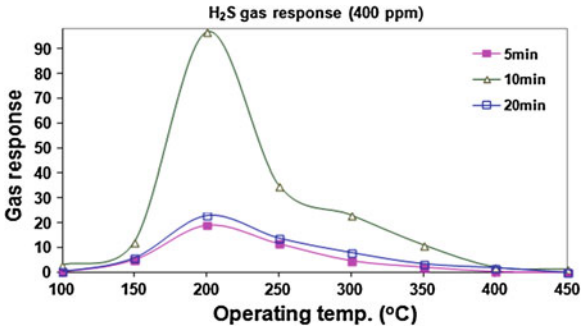

Fig. 12 Variations in response to H_2S gas with operating temperature of cupricated ST_{30} film

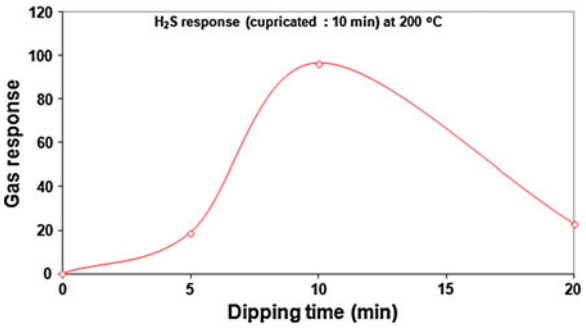

Fig. 13 Variation in H_2S gas response with dipping time of ST_{30} film

the gases selected at 300 °C operating temperatures of pure film and enhances the response to H_2S gas. It is evident that the cupricated sensor was highly selective to H_2S gas at 200 °C.

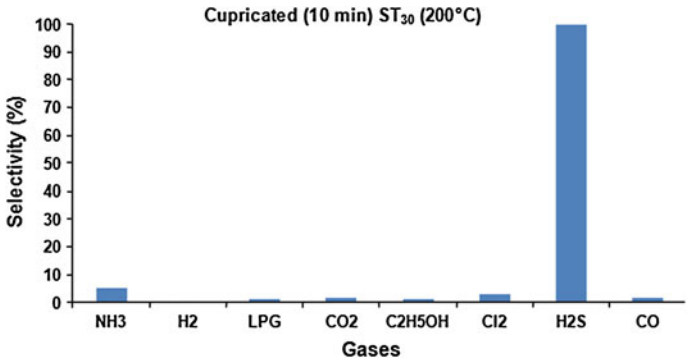

Fig. 14 Selectivity of cupricated ST_{30} film to H_2S against other gases

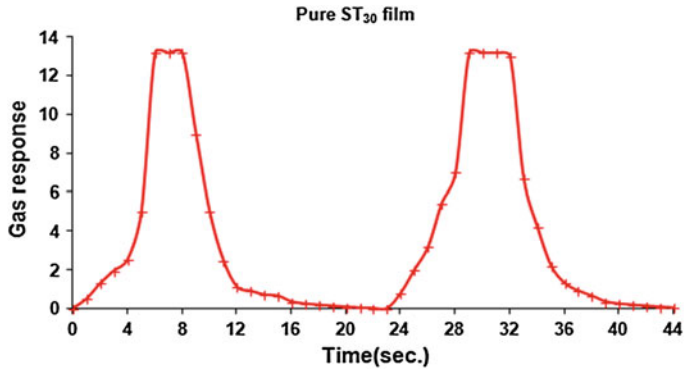

Fig. 15 Response and recovery time of pure ST_{30} film

10 Response and Recovery Time of Sensors

10.1 Pure ST_{30} Film

The response and recovery time of pure ST_{30} film are represented in Fig. 15. The response time of pure ST_{30} film was 5 s. and recovery time was 22 s. at operating temperature 300 °C.

10.2 Cupricated ST_{30} Film

Figure 16 shows the response and recovery time of cupricated (10 min.) ST_{30} film. The response time of the film was 3 s and recovery time was 20 s at operating temperature 200 °C. This indicates that surface cuprication of the film reduces the

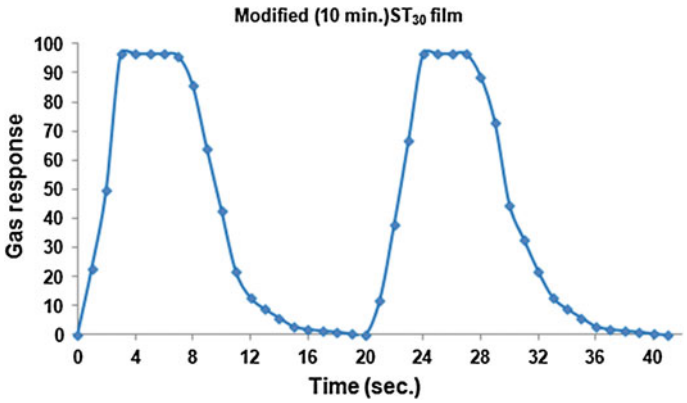

Fig. 16 Response and recovery time of cupricated (10 min) ST_{30} film

response and recovery time of the sensor. The small response and recovery time are the remarkable features of the cupricated ST_{30}.

11 Long-Term Stability of Sensor

11.1 Pure ST_{30} Film

Figure 17 shows the long term stability of pure ST_{30} film. It was observed that the over a long period (2 month) the response of the sensor was found to be nearly same.

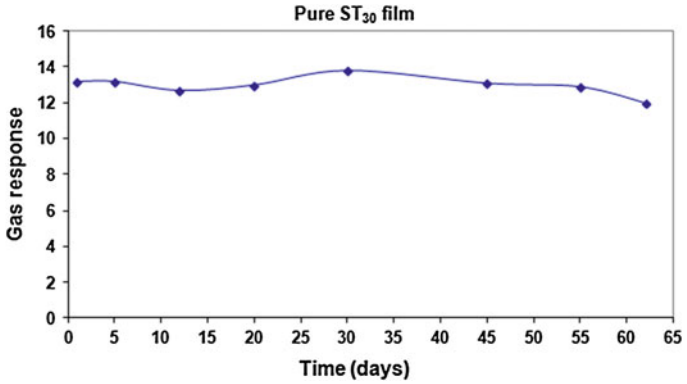

Fig. 17 Long time stability of pure ST_{30} film

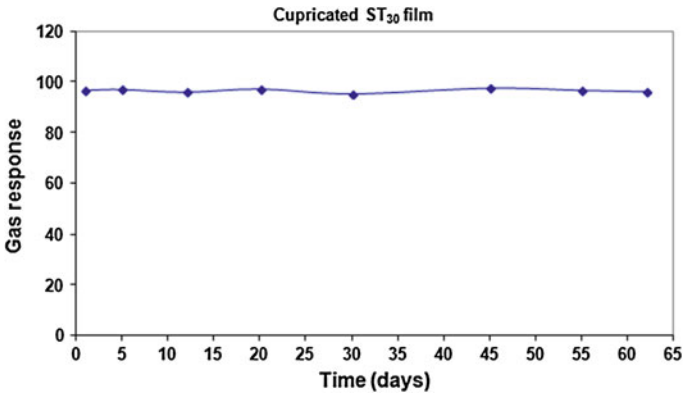

Fig. 18 Long time stability of cupricated (10 min) ST_{30} film

11.2 Cupricated ST_{30} Film

Long term stability of cupricated ST_{30} film is shown in Fig. 18. It was observed that due to cuprication of the films the long time stability of gas response of the sensor is found to be improved.

12 Gas Response to Different Gas Concentrations

Figure 19 exhibits response to H_2S gas for various gas concentrations ranging from 100 to 800 ppm at 200 °C operating temperature. It observed that sensitivity increases linearly from 100 to 400 ppm after that, film shows nearly constant response. This may be due to the masking of sensor surface and not responding further increasing gas concentration. So sensor would be used in active region (100–400 ppm).

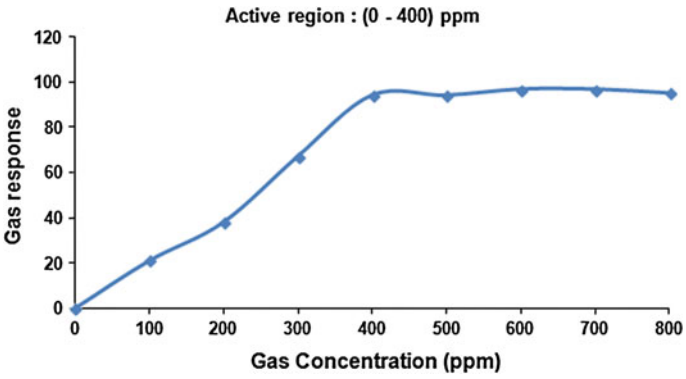

Fig. 19 Response to H_2S gas for different gas concentration of cupricated (10 min) ST_{30} film

13 Error Measurement

The standard deviation (σ) is calculated from the squares of the deviations from the mean using the following formula (7):

$$\sigma = \sqrt{\frac{\sum \left[(x_i - \bar{x})^2\right]}{n-1}} \tag{7}$$

Measurement of % error in gas response of ST_{30} film of pure and most gas sensitive cupricated ST_{30} film is depicted in Table 5.

It is observed that the maximum error is less than 10 %. It means the measurement method carried in this work is correct. It is also observed that error decreases with surface modification that indicates the method of surface modification is correct.

14 Summary Table

Samples	Optimum operating conditions			Gas sensing performance			
	Dipping time	Temp. (°C)	Gas conc. (ppm)	Max. sensitive to gas	Gas response	Res. time (s)	Rec. time (s)
Pure ST_{30} film	–	300	400	CO_2	13.20	6	24
Cupricated ST_{30} film (10 min)	10 min	200	400	H_2S	96.70	3	20

ST_{30} :$(Sn_{0.3}Ti_{0.7})O_2$, Conc.: concentration, Max.: Maximum, Res.: Response, Rec.: Recovery

15 Discussion

Gas response (S) is the device characteristic of perceiving a variation in physical and/or chemical properties of the sensing material under gas exposure. The sensitivity, in the case of resistive gas sensors, is defined as the relative change in

Table 5 Measurement of % error in gas response

Sample	Temp.	Gas response	Standard Deviation (σ)	% Error
Pure ST_{30} film	300	13.20	0.79	6
Cupricated ST_{30} film (10 min.)	200	96.70	0.63	1

resistance of the thick film. It is the ratio of the change in the resistance of the thick film in air to the change in resistance in particular gas atmosphere. The sensitivity is given by (8) [22]:

$$\text{Gas response (S)} = \left|\frac{R_a - R_g}{R_a}\right| = \frac{\Delta R}{R_a} \tag{8}$$

where, R_a–resistance of a thick film sensor in air

R_g–resistance of a thick film sensor in a sample gas

It is the ability of a sensor to respond to a certain gas in presence of other gases is known as selectivity. A good sensor will discern a particular signal by allowing adsorption of the desired gas while remaining insensitive to others.

The % selectivity of 'target gas' to another gas is defined as:

$$\%\text{Selectivity} = \frac{S_A}{S_B} \times 100 \tag{9}$$

where, S_A and S_B are the sensitivities of sensors in 'target gas' and B gas, respectively.

It is known that atmospheric oxygen molecules are adsorbed on the surface of ST_{30} semiconductor oxide in the forms of O^-, $O_2{}^-$ and O^{2-}, thereby decreasing the electronic conduction. Atmospheric oxygen molecules take electrons from the conduction band of ST_{30} to be adsorbed as O^- ST_{30}. The reaction is as follows:

$$O_2\{g\} + 2e^- \rightarrow 2O^- ST_{30} \tag{10}$$

When reducing gas molecules like CO_2 react with negatively charged oxygen adsorbates, the trapped electrons are given back to conduction band of ST_{30}. The energy released during decomposition of adsorbed CO_2 molecules would be sufficient for electrons to jump up into conduction band of ST_{30}, causing an increase in the conductivity of sensor.

For oxidation of CO_2, some amount of activation energy has to be provided thermally. An increase in operating temperature surely increases the thermal energy so as to stimulate the oxidation of CO_2. The reducing gas (CO_2) donates electrons to ST_{30}. Therefore, the resistance decreases, or the conductance increases. This is the reason why the gas response increases with operating temperature. The point at which the gas response reaches maximum is the actual thermal energy needed for the reaction to proceed. However, the response decreases at higher operating temperatures, as the oxygen adsorbates are desorbed from the surface of sensor [28]. Also, at high temperatures the carrier concentration increases due to intrinsic thermal excitation and the Debye length decreases. This may be one of the reasons for the decreased gas response at high temperatures [11].

The interaction between a semiconductor surface and H_2S may be explained in terms of reaction of H_2S molecules with pre-adsorbed oxygen. Oxygen adsorbs at the surface in several forms such as : O^-, $O_2{}^-$ and O^{2-}.

The H_2S gas is reducing in nature. It can reduce CuO into CuS which are metallic in nature and is more conducting. This can be represented as:

$$CuO + H_2S \rightarrow CuS + H_2O \quad (11)$$

Upon subsequent exposure of sensor to air ambient at elevated temperature, sulphides got oxidized and could be recovered back to oxides as

$$2CuS + 4O_2 \rightarrow 2CuO + 2SO_3 \quad (12)$$

When oxygen is adsorbed on the surface of ST_{30} film, abstracting electrons, and thus an increase in potential barrier at the grain boundaries. When reducing gas such as H_2S is adsorbed between the grains of ST_{30} film, the potential barrier decreases as a result of oxidative conversion of the H_2S gas. H_2S reacts with adsorbed oxygen ions as:

$$H_2S + 3O^- \rightarrow H_2O + SO_2 + 3e^- \quad (13)$$

The amount of oxygen adsorbed on the surface of cubricated ST_{30} films is more, since copper oxide form misfit regions between the grains of ST_{30} film and act as efficient catalysts for oxygenation.

When the optimum amount of copper oxide is incorporated on the surface of the ST_{30} film, copper species would be distributed uniformly throughout the surface (Fig. 3b). Due to this not only the initial resistance of the film is high but this amount would also be sufficient to promote the catalytic reaction effectively and the overall change in resistance on exposure of the test gas larger leading to high sensitivity to gas.

When the amount of copper oxide on the surface of the film is less than the optimum, the surface dispersion would be poor and amount may not be sufficient to promote the reaction more effectively leading to decreased sensitivity.

The nonlinearity of the electrical conductivity-temperature profiles of the samples reveals the semiconducting nature of pure and cupricated ST_{30}. The semiconducting nature may be attributed to oxygen deficiencies in ST_{30}. Cupri-cation of ST_{30} has enhanced the electrical conductivity. This may be due to the bridging of intergranular gaps between ST_{30} particles by small particles of CuO segregated around the grain boundaries of ST_{30}.

Fast recovery and response to H_2S gas may be due to faster adsorption–desorption reactions on the surface of the cupricated films. A large number of oxygen ions would be adsorbed on the misfit regions of copper in ambient air. The larger the misfits on the surface, the larger would be the number of oxygen ions adsorbed on the surface leading to high resistance. The larger the number of oxygen ions adsorbed on the surface, the faster would be the oxidation of the exposed gas and the response time. ST_{30} was observed to be highly oxygen deficient. The larger the oxygen deficiency, the faster would be the adsorptions of oxygen ions and in turn the faster the recovery of the sensor.

16 Summary and Conclusions

Following statements can be made from the experimental results.

- The thick films of pure ST_{30} were sensitive to CO_2 gas at 300 °C.
- Surface cuprication process was employed to modify only the surface of the film and not the bulk portion of the base material ST_{30}.
- The thick films of pure and cupricated ST_{30} was observed to be semiconducting in nature and showed a negative temperature coefficient of resistance.
- The cuprication alters morphology and shifts response of the films towards H_2S gas at temperature (200 °C).
- Cupricated films were found to be more porous film. As porosity increases of the film, the gas response of the film would be increases.
- Average crystallite size from XRD using Scherrer formula of pure film was 41 nm.
- Response and recovery time of cupricated film was reduced due to surface modification.
- Cupricated films showed the good long time stability compare to pure film.
- The optical energy band gap of prepared ST_{30} sample was found to be 3.35 eV.

Acknowledgments The author would like to thank UGC (WRO), Pune for the financial support to research work. The authors also thank to university of Pune for the help in the characterization of the films. A special thanks goes to the Principal of the K.T.H.M. College, Nashik for providing the facility of laboratory for research work.

References

1. K. Zakrzewska, Mixed oxides as gas sensors. Thin Sol. Films **391**, 229–238 (2001)
2. R. Moos, A brief overview on automotive exhaust gas sensors based on electroceramics. Int. J. Appl. Ceram. Technol. **2**, 401–413 (2005)
3. W. Schmid, N. Barsan, U. Weimar, Sensing of hydrocarbons with tin oxide sensors: possible reaction path as revealed by consumption measurements. Sens. Actuat. B Chem. **89**, 232–236 (2003)
4. E. Traversa, M. Miyayama, H. Yanagida, Gas sensitivity of ZnO/La_2CuO_4 heterocontacts. Sens. Actuat. B Chem. **17**, 257–261 (1994)
5. J. Tamaki, T. Maekawa, N. Miura, N. Yamazo, Gold-loaded tungsten-oxide sensor for detection of ammonia in air. Sens. Actuat. B Chem. **9**, 197–203 (1992)
6. X. Zhou, Q. Cao, Y. Hu, J. Gao, Y. Xu, Sensing behavior and mechanism of La_2CuO_4-SnO_2 gas sensors. Sens. Actuat. B Chem. **77**, 443–446 (2001)
7. X. Zhou, Q. CaO, H. Huang, P. Yang, Y. Hu, Study on sensing mechanism of CuO–SnO_2 gas sensors. Mater. Sci. Eng. B **99**(1–3), 44–47 (2003)
8. R. Kumar, A. Khanna, P. Tripathi, R. Nandedkar, S. Potdar, S. Chaudhari, S. Bhatti, CuO SnO_2 element as hydrogen sulfide gas sensor prepared by a sequential electron beam evaporation technique. J. Appl. Phys. **36**, 2377–2381 (2003)

9. F. Edelman, H. Hahn, S. Seifried, C. Alof, H. Hoche, A. Balogh, P. Werner, K. Zakrzewska, M. Radecka, P. Pasierb, A. Chack, V. Mikhelashvili, G. Eisenstein, Structural evolution of SnO_2–TiO_2 nanocrystalline films for gas sensors. Mater. Sci. Eng. B **69–70**, 386–391 (2000)
10. M. Radecka, K. Zakrzewska, M. Rgkas, SnO_2–TiO_2 solid solutions for gas sensors. Sens. Actuat. B Chem. **47**, 194–204 (1998)
11. J. Mizsel, How can sensitive and selective semiconductor gas sensors be made? Sens. Actuat. B **23**, 173–176 (1995)
12. L. Kong, J. Ma, H. Huang, Preparation of the solid solution $Sn_{0.5}Ti_{0.5}O_2$ from an oxide mixture via a mechanochemical process. J. Alloy. Compd. **336**, 315–319 (2002)
13. Y. Park, H. Song, C. Lee, J. Jee, Fabrication and its characteristics of metal-loaded TiO_2/SnO_2 thick-film gas sensor for detecting dichloromethane. J. Ind. Eng. Chem. **14**, 818–823 (2008)
14. M. Carotta, A. Cervi, S. Gherardi, V. Guidi, C. Malagu, G. Martinelli, B. Vendemiati, M. Sacerdoti, G. Ghiotti, S. Morandi, S. Lettieri, P. Maddalena, A. Setaro, (Ti, Sn)O_2 solid solutions for gas sensing: a systematic approach by different techniques for different calcination temperature and molar composition. Sens. Actuat. B Chem. **139**, 329–339 (2009)
15. G. Jain, V. Gaikwad, L. Patil, Studies on gas sensing performance of $(Ba_{0.8}Sr_{0.2})(Sn_{0.8}Ti_{0.2})O_3$ thick film resistors. Sens. Actuat. B Chem. **122**, 605–612 (2007)
16. J.D. Lee, *Concise In-organic Chemistry,* 5th edn. (Wiley India, New Delhi, 2008), p. 698
17. G.S. Manku, *In-organic Chemistry* (TMG Co, New York, 1984), pp. 465–467
18. T. Ishihara, K. Kometani, Y. Nishi, Y. Takita, Improved sensitivity of CuO–$BaTiO_3$ capacitive type CO_2 sensor by additives. Sens. Actuat. B Chem. **28**, 49–54 (1995)
19. C.A. Harper, *Hand Book of Thick Film Hybrid Microelectronics* (McGraw-Hill Co, New York, 1974)
20. M. Wagh, L. Patil, T. Seth, D. Amalnerkar, Surface cupricated SnO_2-ZnO thick films as a H_2S gas sensors. Mater. Chem. Phys. **84**, 228–233 (2004)
21. S. Patil, L. Patil, D. Patil, G. Jain, M. Wagh, CuO-modified tin titanate thick film resistors as H_2-gas sensors. Sens. Actuat. B Chem. **123**, 233–239 (2007)
22. G. Jain, L. Patil, Gas sensing properties of Cu and Cr activated BST thick films. Bull. Mater. Sci. **29**, 403–411 (2006)
23. V. Choudhary, I. Mulla, K. Vijaymohan, Comparative Studies of doped and surface modified tin oxide towards hydrogen sensing: synergistic effects of Pd and Ru. Sens. Actuat. B **50**, 45–51 (1998)
24. H. Naidu, A. Virkar, Low-temperature TiO_2–SnO_2 phase diagram using the molten-salt method. J. Am. Ceram. Soc. **81**, 2176–2180 (1998)
25. B. Cullity, *Elements of X-ray Diffraction*, 2nd edn. (Addison Wesley, Reading, 1978), p. 107
26. K. Porkodi, S. Arokiamary, Synthesis and spectroscopic characterization of nanostructured anatase titania: a photocatalyst. Mater. Charact. **58**, 495–503 (2007)
27. Molea, V. Popescu, The obtaining of titanium dioxide nanocrystalline powders. Optoelectron. Adv. Mater. Rapid Commun. **5**(3–4), 242–246 (2011)
28. H. Wndichamann, P. Mark, A model for the operation of a thin film oxide (snOx) conductance-modulation carbon monoxide sensor. J. Electrochem. Soc. **126**, 627–633 (1979)